ELSEVIER

Journal of Quantitative Spectroscopy & Radiative Transfer 100 (2006) 393–405

Journal of Quantitative Spectroscopy & Radiative Transfer

www.elsevier.com/locate/jqsrt

Light scattering by small feldspar particles simulated using the Gaussian random sphere geometry

B. Veihelmann[a,b,*], T. Nousiainen[c], M. Kahnert[d], W.J. van der Zande[a]

[a]*Institute for Molecules and Materials, Radboud University Nijmegen, The Netherlands*
[b]*Earth Oriented Science Department, National Institute for Space Research (SRON), Utrecht, The Netherlands*
[c]*Department of Physical Sciences, Division of Atmospheric Sciences, University of Helsinki, Finland*
[d]*Swedish Meteorological and Hydrological Institute, Norrköping, Sweden*

Abstract

The single-scattering properties of Gaussian random spheres are calculated using the discrete dipole approximation. The ensemble of model particles is assumed to be representative for a feldspar dust sample that is characteristic for weakly absorbing irregularly shaped mineral aerosol. The morphology of Gaussian random spheres is modeled based on a statistical shape analysis using microscope images of the dust sample. The size distribution of the dust sample is based on a particle sizing experiment. The refractive index of feldspar is estimated using literature values. All input parameters used in the light scattering simulations are thus obtained in an objective way based on the true properties of the mineral sample. The orientation-averaged and ensemble-averaged scattering matrices and cross sections of the Gaussian random spheres are compared with light scattering simulations using spheroidal shape models which have been shown to be applicable to the feldspar sample. The Gaussian random sphere model and the spheroidal shape model are assessed using the measured scattering matrix of the feldspar dust sample as a reference. Generally, the spheroidal model with strongly elongated prolate and strongly flattened oblate shapes agrees better with the measurement than the Gaussian random sphere model. In contrast, some features that are characteristic for light scattering by truly irregular mineral dust particles are rendered best by the Gaussian random sphere model; these features include the flat shape of the phase function and a minimum in the scattering matrix element F_{22}/F_{11} as a function of the scattering angle.

PACS: 42.68.−w; 42.68.Jg; 42.68.Mj; 42.68.Wt; 92.60.Mt; 92.60.Vb; 94.10.Gb; 95.75.Hi; 95.75.Rs

Keywords: Light scattering; Irregular; Atmospheric aerosol; Mineral dust; Desert dust; Volcanic ash; Solar radiation; Remote sensing; Polarimetry

1. Introduction

Atmospheric aerosols are monitored with ground-based and satellite-based sensors measuring scattered sunlight [1,2]. An accurate knowledge of the light scattering properties of the aerosol is essential for the

*Corresponding author. Institute for Molecules and Materials, Radboud University Nijmegen, The Netherlands. Fax: +31 30 2203028.
E-mail address: ben.veihelmann@knmi.nl (B. Veihelmann).

0022-4073/$ - see front matter © 2005 Elsevier Ltd. All rights reserved.
doi:10.1016/j.jqsrt.2005.11.053

interpretation of measured intensity and polarization data. In practice, a numerical model is required that describes the single-scattering properties of aerosol as a function of the refractive index, the size distribution, and the shape of the aerosol particles. A large fraction of the aerosol mass present in the Earth's atmosphere is irregularly shaped mineral dust [3]. It has been shown in various studies that neglecting the nonsphericity of mineral aerosol particles can yield large errors in simulated radiances and retrieved aerosol parameters [4–6]. In a recent study it has been shown as well that simulated radiation flux data can be erroneous if irregular aerosol particles are approximated by spheres [7].

In order to take the nonsphericity of mineral aerosol into account in light scattering simulations, shape approximations are used. Irregular aerosol particles may be represented by ensembles of simple nonspherical shapes such as spheroids, prisms, cylinders, or more complex shapes [8]. The single-scattering properties of these model particles must then be calculated using numerical light scattering codes which in general impose constraints on the ensemble of model particles (cf. [9]).

We simulate light scattering by mineral aerosol using the Gaussian random sphere geometry [10]. With this model the morphology of the particles of a feldspar dust sample is modeled statistically (Section 2). This mineral sample is representative for weakly absorbing irregularly shaped mineral dust aerosol. The statistical shape parameters used in the Gaussian random sphere model are extracted from scanning electron microscope (SEM) images of a feldspar dust sample using a method described in Nousiainen et al. [11] and in Nousiainen and McFarquhar [12]. The generated model shapes used in the Gaussian random sphere model have no symmetry. In that sense, the statistical shape model using Gaussian random spheres is more representative for natural irregular particles than shape models using spheroids which are rotationally symmetric. We use the discrete dipole approximation (DDA) to calculate the orientation-averaged scattering matrix and the cross sections for scattering and absorption (for definitions see [8]) of the model particles at a wavelength of $\lambda = 632.8\,\text{nm}$ (Section 3).

Nousiainen et al. [11] have simulated light scattering by Gaussian random spheres representing large Saharan dust particles with a modified ray-optics approximation. Due to the limitations of the modified ray-optics approximation, this study accounts for model particles representing large soil-derived airborne particles in dust storms with volume-equivalent sphere radii of $r_v \geqslant 2\,\mu\text{m}$. In the study presented here we consider small feldspar particles that are representative for tropospheric aerosol in background conditions. The light scattering simulations presented here are made without using optimizations regarding the shape, the refractive index, or the size distribution.

Feldspar is a silicate that is very abundant in the Earth's crust. This mineral occurs in the forms of alkali-feldspar and plagioclase and has pronounced cleavage planes [13]. The feldspar sample studied here originates from grinding a bulk crystal. The size distribution of this sample is estimated based on a light scattering measurement using a laser particle sizer. The estimates for the effective radius and the effective variance are $r_{\text{eff}} = 1.0\,\mu\text{m}$ and $v_{\text{eff}} = 1.0$, respectively (for definition see [14]). The refractive index of feldspar is estimated to be $m = 1.57 - 0.0005\text{i}$. The real part is taken from Huffman [15] while the imaginary part is adopted from other weakly absorbing silicate minerals (mica) [16]. The feldspar sample can be considered representative for weakly absorbing atmospheric mineral aerosol [17–19].

The scattering matrices $\mathbf{F}$ of the feldspar sample and various other irregularly shaped mineral dust samples have been measured with a so-called nephelometer experiment [20,21]. The scattering matrix elements $F_{ij}(\Theta)$ of dust samples are measured as a function of the scattering angle in the range from $\Theta = 5^\circ$ to 173° at the wavelengths $\lambda = 441.6$ and $632.8\,\text{nm}$. The scattering angle Θ is defined as the angle between incoming and scattered beams, whereas $\Theta = 0^\circ$ denotes forward scattering. The nephelometer experiment is set up such that the scattering particles are randomly oriented [20]. The scattering matrix of the feldspar sample measured at $\lambda = 632.8\,\text{nm}$ is used as a reference for the light scattered simulations presented in this study.

A widely used approach is to represent irregular aerosol particles by an ensemble of rotationally symmetric spheroids with various aspect ratios. The aspect ratio $\varepsilon = a/b$ is defined by the length of the symmetry axis b and the length of an axis a that is orthogonal to the symmetry axis. The single-scattering properties of small spheroidal particles can be calculated using the T-matrix code [22]. Nousiainen and Vermeulen [23] have compared T-matrix calculations for a mixture of prolate and oblate spheroids with the feldspar measurement. An equiprobable shape distribution is used, i.e. particles with different aspect ratios are assumed to be present in equal numbers. Based on the same reference measurement, Veihelmann et al. [24] have investigated the

impact of shape approximations on polarimetric satellite observations including their sensitivity with respect to the optical thickness and the single-scattering albedo of the aerosol. Recently, Nousiainen et al. [25] have derived optimal estimates as well as a practical parameterization for the aspect ratio distribution based on the feldspar measurement. Kahnert et al. [26] applied this parameterization as well as the measured phase function of the feldspar sample for atmospheric radiance and flux simulations in the visible.

The conclusion of these studies is that the spheroidal shape approximation constitutes a major improvement over the spherical shape approximation for the simulation of light scattered by irregular particles. The agreement between measured and simulated scattering matrices depends critically on the aspect ratio distribution. Optimal estimates for the aspect ratio distribution derived by Nousiainen et al. [25] for the feldspar sample strongly weight the more extreme spheroids while the weight of the nearly spherical shapes is reduced. However, systematic differences remain between the measured scattering matrices and the simulations based on the spheroidal shape approximation. These discrepancies may be related to the symmetry of the model particles which is not found for natural mineral aerosol particles. The discrepancies may as well be due to the absence of inhomogeneities in the model particles, or to the absence of small scale structures in the shapes of the model particles.

We investigate the agreement and the differences between the Gaussian random sphere model and the spheroidal shape approximation (Section 4). For this purpose, we compare the simulations for Gaussian random spheres using the discrete dipole approximation with T-matrix calculations for ensembles of prolate and oblate spheroids with the same refractive index and the same particle volume. For the shape averaging we use parameterized shape distributions including a parameterization that was found to be appropriate for the feldspar sample [25]. In Section 5 we compare the results of the Gaussian random sphere model and the spheroidal models for individual size classes.

The simulated scattering matrices are size-averaged using the size distribution of the feldspar sample. With the DDA calculations we include about 86% of the total scattering cross section of the feldspar sample. With the simulations for spheroidal particles 97% of the total effective scattering cross section is accounted for. We merge the DDA simulations for Gaussian random spheres with radii r_v ranging from 0.1 to 1.3 μm with T-matrix simulations for spheroids with radii r_v ranging from 1.3 to 2.6 μm. This enables us to assess the Gaussian random sphere model and the spheroidal model using the measured scattering matrix of the feldspar sample as a reference (Section 6).

2. Gaussian random sphere geometry

Natural mineral aerosol particles are irregular in the sense that there is no simple function that could describe their shape. We use the Gaussian random sphere geometry [10,27] to model the statistical properties of the shapes of the feldspar dust sample. The Gaussian random sphere is a statistical shape described by the radius r as a function of the spherical coordinates θ and ϕ

$$r(\theta,\phi)=\frac{a}{\sqrt{1+\sigma^2}}\exp(s(\theta,\phi)) \tag{1}$$

and depends on the mean radius a, the relative standard deviation of the radius σ, and the logradius s

$$s(\theta,\phi)=\sum_{l=0}^{\infty}\sum_{m=-l}^{l}s_{lm}Y_{lm}(\theta,\phi) \tag{2}$$

which is the sum of spherical harmonic functions Y_{lm}

$$Y_{lm}(\theta,\phi)=\sqrt{\frac{2l+1}{2}\frac{(l-m)!}{(l+m)!}}P_{lm}(\cos(\theta))\mathrm{e}^{\mathrm{i}m\phi} \tag{3}$$

that are weighted with the complex coefficients s_{lm}. P_{lm} denote the associated Legendre functions. The complex coefficients s_{lm} have zero mean values and a variance

$$\mathrm{Var}(\mathrm{Real}(s_{lm}))=(1+\delta_{m0})\frac{2\pi}{2l+1}C_l, \tag{4}$$

$$\mathrm{Var}(\mathrm{Imag}(s_{lm})) = (1-\delta_{m0})\,\frac{2\pi}{2l+1}\,C_l \tag{5}$$

for $l = 0, 1, 2, \ldots, \infty$ and $m = -l, \ldots, l$ (see [27]). The Kronecker delta δ_{mn} is unity for $m = n$ and zero otherwise. Note that the variance of the coefficients s_{lm} depends only on the coefficient C_l of the same degree l.

The coefficients C_l are related to the covariance function $\Sigma_r(\gamma)$ of the radius r expressed as a function of the angular distance γ between two directions (θ_1, ϕ_1) and (θ_2, ϕ_2). The covariance function of the radius is a measure of the particle morphology. Naturally, the covariance function $\Sigma_r(\gamma)$ of a sphere is a constant. For nonspherical shapes Σ_r has a maximum at $\gamma = 0$. The smaller the scale of the shape features, the faster $\Sigma_r(\gamma)$ drops with increasing angle γ from its maximum value $\Sigma_r(0) = \sigma$. The covariance function Σ_r of the radius is related to the covariance function of the logradius Σ_s

$$\Sigma_s = \ln(\Sigma_r + 1), \tag{6}$$

which can be expanded in a series of Legendre functions

$$\Sigma_s(\gamma) = \sum_{l=0}^{\infty} C_l P_l(\cos(\gamma)). \tag{7}$$

The sum of the coefficients C_l equals the variance of the logradius β^2, viz.

$$\sum_{l=0}^{\infty} C_l = \beta^2 = \ln(1+\sigma^2). \tag{8}$$

By analogy with the concepts used in Fourier analysis, the coefficients C_l can be regarded as a power spectrum of the logradius. The shape of a Gaussian random sphere is isotropic in the sense that the covariance function of a Gaussian random sphere is independent of the orientation of the intersection. That is why an ensemble of generated Gaussian random sphere realizations is randomly oriented.

We generate a finite ensemble of Gaussian random sphere realizations with shape statistics that are representative for the feldspar sample following the approach described in Nousiainen et al. [11] and in Nousiainen and McFarquhar [12]. We determine the covariance function $\Sigma_r(\gamma)$ of an ensemble of feldspar particles in order to obtain an estimate for the statistical properties of the feldspar particles. The particle intersections of the feldspar particles cannot be measured with the devices available. Instead, we analyze the particle projections taken from scanning electron microscope (SEM) images. A microscope image of the feldspar sample showing very large particles has been published by Volten et al. [20]. The images used in the shape analysis show particles with irregular shapes as well as particles with sharp edges and planar surfaces. Most particles, for which the 3D shape can be guessed, exhibit no apparent preferential orientation. Therefore we assume that the morphology statistics extracted from 2D projections is representative for the ensemble of 3D particles. The radius $r(\gamma)$ of the projections of more than 200 particles is evaluated. The morphology of the feldspar sample is now captured in terms of the ensemble-average of the series of coefficients C_l. The coefficients C_l extracted from the SEM images of the feldspar sample follow reasonably well the power law relation $C_l \propto l^{-\nu}$ with $\nu = 2.5$. We obtain a value of 0.2 for the parameter σ. A morphology analysis of a Saharan dust sample yields a similar power law relation with the parameter $\nu = 4$ [11]. According to the exponent ν, the Saharan dust particles have less sharp edges than the feldspar particles. This finding is in agreement with the shapes observed on microscope images of both dust samples.

A part of the information regarding the fine structure of the particle surfaces is lost when using the particle projections instead of the particle intersections. This is partly due to shadowing effects. Therefore, we cannot extract the high-degree Legendre coefficients C_l from the particle projections. We assume the power law relation mentioned above to be applicable up to the degree $l_{\max} = 15$. Including even higher degree contributions has very little impact on the particle shape.

The coefficients s_{lm} in Eq. (2) with $l = 0$ and 1 are mainly responsible for a variation of the particle volume. These coefficients are set to zero in order to generate an ensemble of Gaussian random sphere realizations with a controlled volume. The remaining variance of the particle volume is small and acceptable for our purposes.

The ensemble-averaged volume $\langle V \rangle$ is [28]

$$\langle V \rangle = \tfrac{4}{3} a^3 \exp[3 \ln(\sigma^2 + 1)]. \tag{9}$$

With the parameter $\sigma = 0.2$, the ensemble of generated Gaussian random sphere realizations has a very narrow distribution with an effective radius of $r_{\text{eff}} = 1.04a$ and an effective variance of about $v_{\text{eff}} = 0.0002$.

Due to the statistical nature of the Gaussian random sphere model the relative phases of the spherical harmonic functions are not taken into account. Therefore, this shape model does not render sharp edges and flat surfaces. A comparison of light scattering simulations for polyhedral prisms and spheroids dedicated to the feldspar sample [25] shows that the presence of sharp corners and plane surfaces is not very important for its light scattering properties. Therefore, we consider the Gaussian random sphere model well suited for light scattering simulations of the feldspar sample.

3. Light scattering by Gaussian random spheres

We have tested two numerical codes for the calculation of the single-scattering properties of Gaussian random spheres with linear dimensions comparable to the wavelength. This includes the code DDSCAT 6.1 which is based on the discrete dipole approximation [29], and SScaTT which is based on computing the T-matrix with the null-field method using discrete sources [30]. The convergence of the calculations using SScaTT turned out to be sensitive with respect to the particle shape, especially for the larger particles. We were able to compute a larger range of particle sizes with DDSCAT. That is why we chose the discrete dipole approximation for the light scattering calculations based on the Gaussian random sphere model.

In the discrete dipole approximation the target is replaced by an array of dipoles with a chosen polarizability. The electro-magnetic response of each dipole is determined as a function of the external field and the fields scattered by all other dipoles [31]. Targets are generated as 3D arrays of dipoles with a Gaussian random sphere realization as an envelope [10]. The elements of the scattering matrix are calculated accurately (with errors less than a few %) if the condition

$$|m| \frac{2\pi}{\lambda} d < 0.5 \tag{10}$$

is satisfied [32]. This poses an upper limit to the lattice spacing d of the dipole array. The required number of dipoles for a spherical particle with a given radius and a refractive index, $m = 1.57 - 0.001\text{i}$, can be estimated by

$$N \approx 100 \cdot x^3, \tag{11}$$

where $x = 2\pi r_{\text{v}}/\lambda$ is the size parameter. The largest particle size we can take into account is therefore limited by the internal memory of the computers used, and by the computing time that increases dramatically with increasing number of dipoles.

The light scattering problem is solved for 196 target orientations. The scattering matrices, the scattering efficiency and the absorption efficiency are averaged over all orientations. The scattering matrices of all shapes in each size class are averaged using the scattering cross sections as weight. Measured scattering matrices of large ensembles of natural irregular shapes have a block diagonal form. This indicates that the measured particle ensemble has no chirality, as it is the case when particles and mirror particles are present in equal numbers. For each model particle of the ensemble we include as well the mirror particle. With this we ensure that the ensemble of Gaussian random sphere realizations with a limited number of individual shapes with no plane of symmetry has no chirality. For size classes with a volume-equivalent radius $r_{\text{v}} \leqslant 1\,\mu\text{m}$ we include 50 pairs of particles and mirror particles. For the size classes with larger radii, not more than 10 particles are used due to computation time reasons. With the computational resources available, the light scattering by particles with volume-equivalent radii up to 1.3 μm are simulated at a wavelength of $\lambda = 632.8\,\text{nm}$. In total, we have invested more than six months of computing (CPU) time in the DDA calculations.

All scattering matrices that were obtained in this work have been tested for consistency. The Cloude test is satisfied for all scattering angles [33]. The conditions for the scattering angles 0° and 180° given by Hovenier and van der Mee [34] are also satisfied.

4. Spheroidal shape approximation

The widely used spheroidal shape approximation is used to put the results of the Gaussian random sphere model into context. The scattering matrix and the cross sections for scattering and extinction of an ensemble of randomly oriented spheroids are calculated using the T-matrix code developed by Mishchenko [22]. This code is based on calculating the T-matrix using the null-field method. The spheroidal shapes can be characterized by the shape parameter ξ

$$\xi = \begin{cases} \varepsilon - 1 : \varepsilon \geqslant 1 & \text{(oblate)}, \\ 1 - \frac{1}{\varepsilon} : \varepsilon < 1 & \text{(prolate)}, \end{cases} \tag{12}$$

where ε of an oblate (prolate) spheroid is defined as the ratio of the major to the minor (minor to major) axis length. Following Nousiainen et al. [25], a parameterized shape distribution $h_n(\xi)$ is used for the shape averaging

$$h_n(\xi) = \begin{cases} C|\xi^n| : & \xi_{\min} \leqslant \xi \leqslant \xi_{\max}, \\ 0 : & \text{otherwise}, \end{cases} \tag{13}$$

where C is a normalization constant. This shape distribution gives more weight to the extreme aspect ratios with increasing parameter n. We consider spheroidal shape models with the equiprobable shape distribution with $n = 0$, and the shape distributions with $n = 1$ and $n = 3$. In the following, these shape approximations will be referred to as spheroidal-ξ^n models. The shape distribution of the spheroidal-ξ^3 models strongly weights the extreme aspect ratios while the near-spherical shapes are suppressed. The value $n = 3$ was found to be appropriate for the feldspar sample [25]. We include spheroids with shape parameters ξ ranging from -2 to 2 in equidistant steps. This corresponds to aspect ratios ε between $\frac{1}{3}$ and 3.

5. Size-specific results

The single-scattering properties simulated using the Gaussian random sphere model are compared with simulations using spheroidal models with various shape distributions. We compare the simulations for particles with the same volume. This is a commonly used approach for small particles with typical dimensions smaller than the wavelength. The surface area is more appropriate for describing the size of larger particles (e.g. [8]). In this study we consider size distributions that include significant contributions in both size domains. It is desirable to characterize consistently the size of all particles. To this end, we chose the particle volume since the surface area of the Gaussian random spheres is much more difficult to determine. Light scattering calculations are made for 22 size classes with radii ranging from $r_v = 0.01\,\mu\text{m}$ to $r_v = 1.3\,\mu\text{m}$ at a wavelength of $\lambda = 632.8\,\text{nm}$. The radii are evenly spaced on a logarithmic scale. The T-matrix simulations for spheroids are made for narrow log-normal size distributions with the same effective radii and variances. We simulate the light scattering by spheroidal particles for size classes with effective size parameters x ranging from 0.01 to 26.

In Fig. 1 we show the simulated scattering cross sections c_{scat} in terms of the scattering efficiency $Q_{\text{scat}} = c_{\text{scat}}/(\pi r_v^2)$ (upper graph) and the asymmetry parameter g (lower graph) as a function of the size parameter x. The results from the Gaussian random sphere model (thick solid) are compared with results from the spheroidal models with $n = 0$ (thin solid), $n = 1$ (thin dashed). The asymmetry parameter g

$$g = \langle \cos(\Theta) \rangle = \frac{\int_0^\pi \cos(\Theta)\sin(\Theta)F_{11}(\Theta)\,\mathrm{d}\Theta}{\int_0^\pi \sin(\Theta)F_{11}(\Theta)\,\mathrm{d}\Theta} \tag{14}$$

is the average cosine of the scattering angle. This parameter is used in radiation flux simulations. The higher its value the more light is scattered into directions with $\Theta < 90^\circ$. Its value equals zero if scattering is symmetric with respect to the scattering angle $\Theta = 90^\circ$. The asymmetry parameters and the scattering efficiency Q_{scat} of all shape models coincide for size parameters up to $x = 4$. For sizes close to $x = 7$, the spheroidal models predict a larger scattering efficiency than the Gaussian random sphere model. In the size range with $5 < x < 10$,

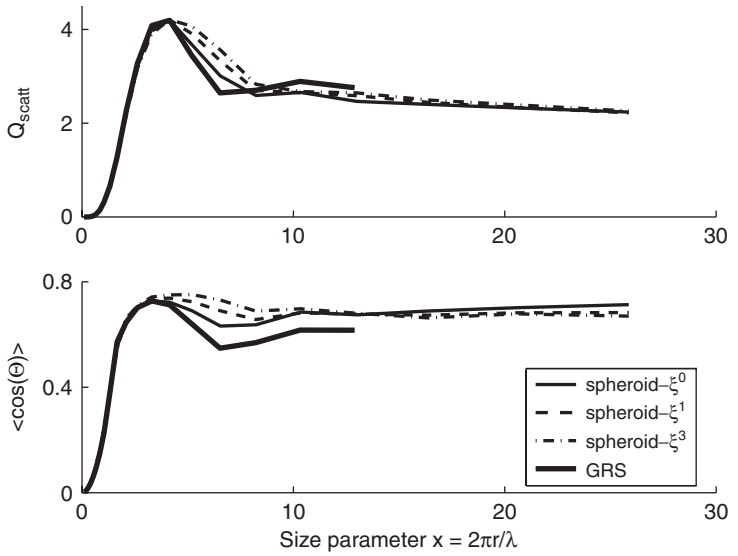

Fig. 1. Simulated scattering efficiency Q_{scat} and asymmetry parameter $g = \langle \cos(\Theta) \rangle$ for Gaussian random spheres (thick solid) and mixtures of prolate and oblate spheroids (thin lines) with the shape distributions ξ^0 (solid), ξ^1 (dashed), and ξ^3 (dash-dotted).

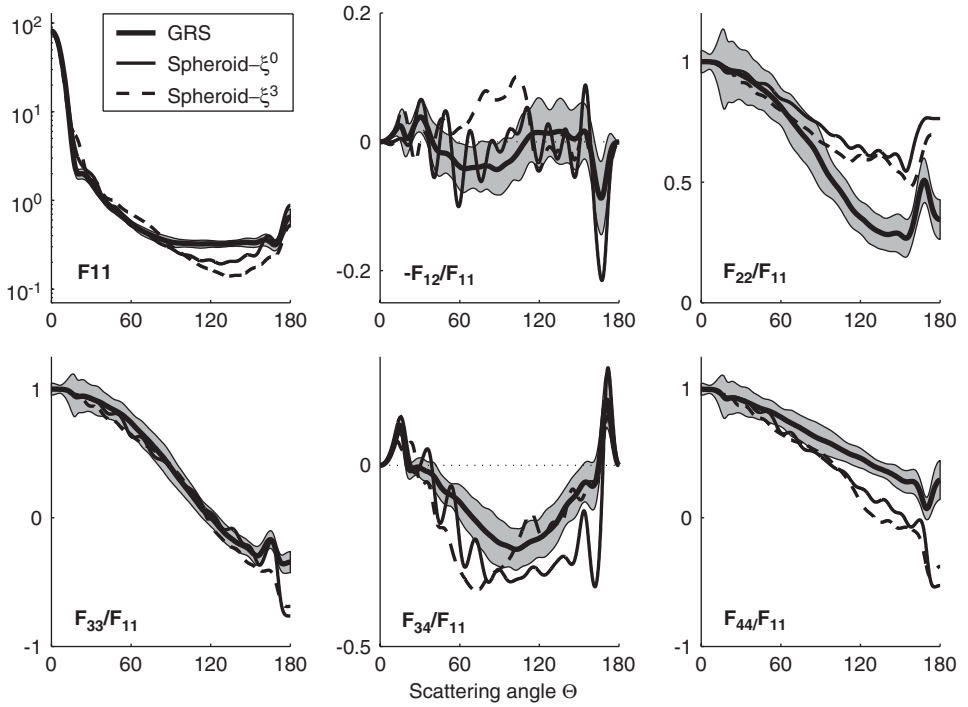

Fig. 2. Simulated scattering matrix using the Gaussian random sphere model (thick solid), the spheroidal-ξ^0 model (thin solid), and the spheroidal-ξ^3 model (dashed) for particles with $x = 10$ and $m = 1.57 - 0.0005\mathrm{i}$. The gray shaded areas depict the $1 - \sigma$ environment of the matrix elements of 100 Gaussian random sphere realizations.

the scattering efficiency of the spheroidal model with $n = 0$ fits best to the results of the Gaussian random sphere model. The same holds in the size range $5 < x < 8$ for the asymmetry parameter.

In Fig. 2 the non-zero elements of the simulated scattering matrices of particles with a size parameter $x = 10$ are depicted as a function of the scattering angle Θ. We show the average (thick solid lines) and the variation

of scattering matrices of the ensemble of 100 Gaussian random sphere realizations in one size class. The gray shaded areas indicate the $1-\sigma$ environment of the matrix elements of the ensemble. Note that the phase function $F_{11}(\Theta)$ is plotted on a logarithmic scale and is normalized using the condition

$$\frac{1}{2}\int_0^{\pi} \sin(\Theta)F_{11}(\Theta)\,\mathrm{d}\Theta = 1. \tag{15}$$

The scattering matrices of the spheroidal models with $n=0$ (thin solid) and $n=3$ (thin dashed) are included. The differences between the scattering matrices of the spheroidal models and the Gaussian random sphere model exceed the standard deviations in all elements at various scattering angles. The differences between the shape models are therefore regarded as significant. Note that the phase function close to 140° of the Gaussian random sphere model exceeds the phase functions of the spheroidal-ξ^3 model by a factor up to 2.

The differences between the scattering matrices of the Gaussian random sphere model and the spheroidal model depend on the size parameter, the shape distribution used in the spheroidal model, the matrix element, and the scattering angle. In Fig. 3 the elements $F_{11}(\Theta)$, $F_{12}(\Theta)/F_{11}(\Theta)$, and $F_{22}(\Theta)/F_{11}(\Theta)$ of simulated scattering matrices are shown. We include results of the Gaussian random sphere model (thick solid), the spheroidal-ξ^0 model (thin solid), and the spheroidal-ξ^3 model (thin dashed) for the size parameters of $x_v = 1.7$, 4.1 and 12.8. The simulated scattering matrices of particles with a size parameter close to $x = 0.1$ are similar to the scattering matrix of Rayleigh scattering. For these particle sizes, the scattering matrices of Gaussian random spheres and spheroids coincide. The Gaussian model and the spheroidal model agree well in the phase function F_{11} at scattering angles close to the forward scattering direction for all particle sizes considered. For $x>2$, the phase function of the spheroidal-ξ^3 model has lower values than the phase function of the Gaussian random sphere model in the range of scattering angles $100° < \Theta < 150°$. In this range of scattering angles, the

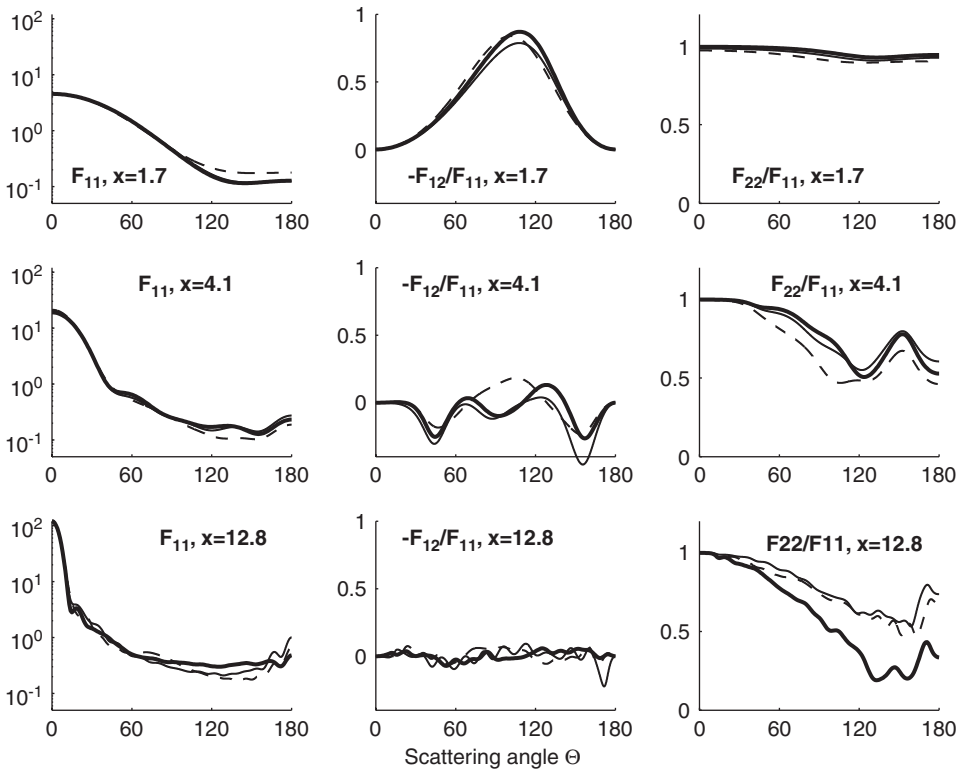

Fig. 3. Phase function (F_{11}) and the elements F_{12}/F_{11} and F_{22}/F_{11} of the simulated scattering matrix using the Gaussian random sphere model (thick solid), the spheroidal-ξ^0 model (solid), and the spheroidal-ξ^3 model (dashed) for the size parameters $x = 1.7$, $x = 4.1$, and $x = 12.8$.

phase functions differ by a factor of up to 1.5 ($x = 1.7$), 1.7 ($x = 4.1$), and 2 ($x = 12.8$). The largest differences in $-F_{12}/F_{11}$ between the Gaussian random sphere model and the spheroidal-ξ^3 model are observed for size parameters close to $x = 2$ (not shown). The spheroidal models show a similarity with the Gaussian random sphere model in the shape of $-F_{12}/F_{11}$ for size parameters up to $x = 6.5$ (not shown). All models considered predict $-F_{12}/F_{11}$ to show decrease in amplitude and to exhibit more peaks and dips with increasing particle size.

The element F_{22}/F_{11} at angles $\Theta > 60^\circ$ is known to be very sensitive with respect to the particle nonsphericity. For spherical particles, F_{22}/F_{11} is unity for all scattering angles. The values of F_{22}/F_{11} decrease with increasing nonsphericity especially in the range of scattering angles from 100° to 160°. For size parameters $x < 2.6$, the Gaussian random sphere model predicts higher values than the spheroidal models. The opposite is true for large particle sizes (see size parameter $x = 12$). For small particles with $x < 4$, the low values of F_{22}/F_{11} appear to be a measure for the global oblateness or prolateness of the shapes rather than for the fine structure of the particle shapes. In summary, we note that the spheroidal model with $n = 0$ agrees better with the Gaussian random sphere model than the spheroidal-ξ^3 model regarding the simulated scattering matrix in the size range between $x = 1$ and $x = 6$. For larger sizes, the differences between the Gaussian random sphere model and the spheroidal models have a similar amplitude as the differences between the spheroidal-ξ^0 and the spheroidal-ξ^3 models.

The differences between the scattering matrices of individual sizes simulated using the various models are large enough to affect radiative transfer simulations (for comparison see [26]). A comparison of the models with an independent objective reference is therefore relevant.

6. Size-averaged results

In order to compare the simulated scattering matrices with the feldspar measurement, the simulations are size-averaged using the size distribution of the feldspar sample. We use a log-normal size distribution with an effective radius $r_{\text{eff}} = 1\,\mu\text{m}$ and an effective variance $v_{\text{eff}} = 1$. As discussed in Section 3, the light scattering simulations for Gaussian random spheres are confined to volume-equivalent sphere radii smaller than $r_v \leqslant 1.3\,\mu\text{m}$. Therefore, it is important to estimate the fraction of the total scattering cross section of the dust sample that is accounted for by the simulations. To this end, the scattering cross section of spheroidal particles with the spheroidal-ξ^3 model are determined for a large range of particle sizes. The cross sections of spheroids with aspect ratios ranging from $\frac{1}{3}$ to 3 and with volume-equivalent sphere radii up to 100 μm are calculated using a light scattering model developed by Min et al. [35]. In this way, the total scattering cross section of the entire distribution can be compared to the total cross section of truncated size distributions. Using the Gaussian random sphere model we account for 86% of the total scattering cross section of the feldspar sample. With the spheroidal models, particles with volume equivalent sphere radii up to 2.6 are included. With this, 97% of the total scattering cross section of the sample is taken into account.

We investigate whether the simulations of light scattering by Gaussian random spheres can be extended to larger particle sizes using the ray-optics approximation (ROA). To this end, scattering matrices of Gaussian random spheres with a size parameter $x = 26$ are calculated using the ray-optics approximation. This approximation is applicable to weakly absorbing spherical particles with size parameters $x \geqslant 80$ [36]. This size limit is expected to decrease with increasing nonsphericity of the scatterers. A comparison of simulations with various models for the size parameters $x = 13$ and $x = 26$ indicates that the ROA provides useful values for the phase function for Gaussian random spheres with size parameter of $x = 26$ (Fig. 4). The phase functions of spheroids with the size parameters $x = 13$ (dotted) and $x = 26$ (dashed) are very similar except for scattering angles close to $\Theta = 0$. The same is true for DDA calculations for Gaussian random spheres with a size parameter $x = 13$ (thin solid) and ROA calculations for Gaussian random spheres with a size parameter $x = 26$ (thick solid). The phase functions of the Gaussian random spheres are significantly flatter than the phase functions of the spheroidal particles for both size parameters. The phase function of particles in this size range appears to be rather insensitive with respect to the particle size. Based on this notion we may conclude that ROA calculations for the phase function at a size parameter $x = 26$ capture the features that are characteristic for the Gaussian random sphere geometry. For the other scattering matrix elements, the comparison of the scattering matrices does not provide the basis for a conclusive statement of this kind.

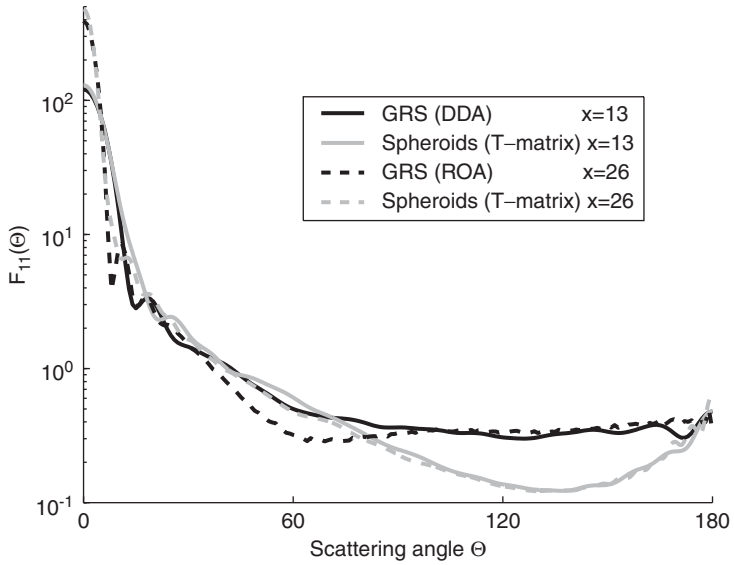

Fig. 4. Simulated phase functions (F_{11}) using DDA for Gaussian random spheres with $x = 13$ (dash-dotted), ROA for Gaussian random spheres with $x = 26$ (solid), and the spheroidal-ξ^3 model for $x = 13$ (dashed) and $x = 26$ (dotted).

The feldspar sample has only a negligible fraction of the total scattering cross section in the size range where it is known for sure that ROA simulations produce reliable results for the entire scattering matrix. That is why the DDA simulations for Gaussian random spheres are extended to larger sizes using the results of the spheroidal-ξ^3 model. An effective scattering matrix is considered that comprises contributions from Gaussian random spheres with volume-equivalent sphere radii $r \leqslant 1.3\,\mu m$ and from spheroids with radii between 1.3 and 2.6 μm. Another valid approach would be to compare the DDA simulations for Gaussian random spheres directly with the measured scattering matrix keeping in mind that 14% of the total scattering cross section of the sample is not accounted for in the simulations. Both approaches are practically equivalent, since the merged scattering matrix is very similar to the result using the Gaussian random sphere model with the truncated size distribution.

In Fig. 5 we compare the merged scattering matrix (thick solid) with the results of the spheroidal-ξ^0 model (thin solid), the spheroidal-ξ^3 model (thin dashed), and the measurement (gray with black dots). In order to apply the normalization (see Eq. (15)) to the measured phase function, the measured data have been extended to the full range of scattering angles as explained in Liu et al. [37]. The phase function of the Gaussian random sphere model is flat in the range of scattering angles from 100° to 170°. This is characteristic for phase functions of irregular mineral particles and has been observed in many measurements of mineral dust samples [38]. The simulated phase functions of the spheroidal models show a broad dip with a minimum between $\Theta = 120°$ and 140°. The Gaussian random sphere model and the spheroidal-ξ^0 model overestimate the phase function for scattering angles $\Theta > 60°$. Close to $\Theta = 150°$ both models overestimate the phase function by a factor of about 1.7. A variation of the size distribution shows that this overestimation cannot be caused by an error in the size distribution alone. None of the models tested here captures the large values of the element $-F_{12}/F_{11}$ in the sideward scattering directions. For the element $-F_{12}/F_{11}$, the result of the Gaussian random sphere model lies between the results of the spheroidal models at most scattering angles. Note that the simulated values of F_{22}/F_{11} using the Gaussian random sphere model are close to the measured values, especially in the range of scattering angles from 120° and 160°. In this respect, the nonsphericity of the Gaussian random spheres appears to be adequate for the feldspar dust sample.

The differences between the scattering matrix of the Gaussian random sphere model and the results from the spheroidal models are on the same order of magnitude as the differences between the results from the spheroidal models. The best agreement with the measured phase function could be achieved with the spheroidal-ξ^3 model. This is true for the phase function, for $-F_{12}/F_{11}$ in the sideward scattering directions,

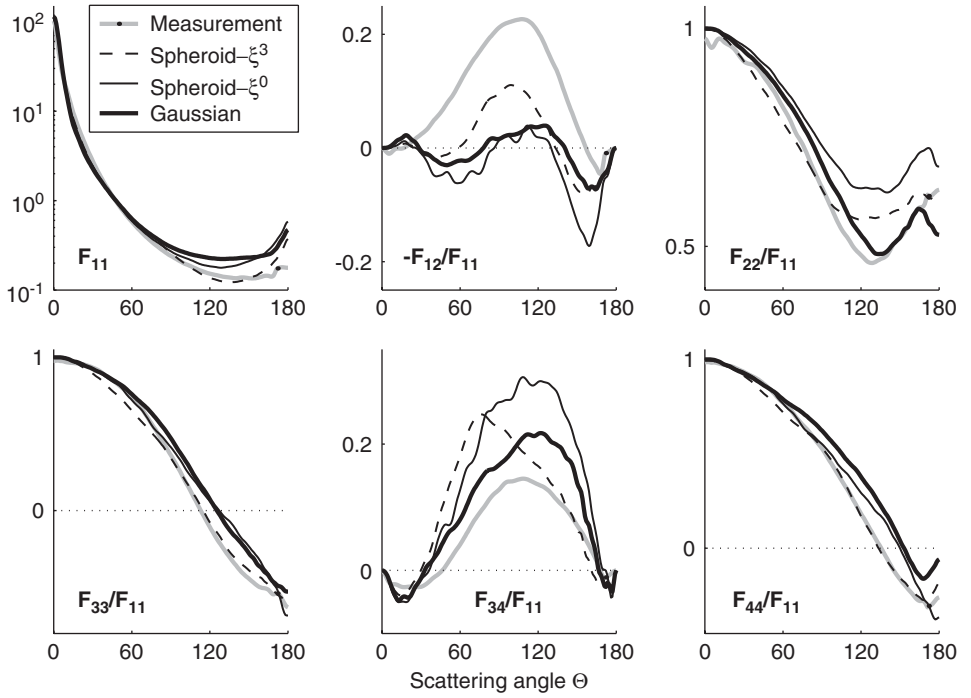

Fig. 5. Size-averaged scattering matrices using the Gaussian random sphere model (thick solid), the spheroidal-ξ^0 model (thin solid), and the spheroidal-ξ^0 model (thin dashed) compared with the measured scattering matrix (gray with black dots).

F_{22}/F_{11} at scattering angles $\Theta \leqslant 110^\circ$, F_{33}/F_{11} and F_{44}/F_{11}. The Gaussian random sphere model shows a better agreement with the measurement only for F_{22}/F_{11} at $120^\circ < \Theta < 160^\circ$ and F_{34}/F_{11} at $40^\circ < \Theta < 100^\circ$.

7. Conclusions

The single-scattering properties of an ensemble of Gaussian random spheres are calculated using the discrete dipole approximation. We assume that the ensemble of Gaussian random spheres is representative for a feldspar dust sample regarding the morphology, the refractive index, and the size distribution. The results are considered to be relevant for weakly absorbing mineral aerosol. The morphology of the Gaussian random spheres is modeled based on microscope images of the mineral dust sample. The size distribution of the dust sample is based on a particle sizing experiment. The refractive index of feldspar is estimated using literature values. All input parameters are thus obtained in an objective way based on the true properties of the mineral sample. With the computational resources available, light scattering simulations for sizes parameters up to $x = 13$ are made. With this 84% of the total scattering cross section of the feldspar sample is taken into account.

We include light scattering simulations using spheroidal model shapes in order to put the results of the Gaussian random sphere model in relation. We consider a spheroidal model with an equiprobable aspect ratio distribution (spheroidal-ξ^0 model). Such shape distributions are often used in light scattering simulations for mineral dust. We also include a parameterization based on shape distributions that are optimized by fitting simulations to the feldspar measurement (spheroidal-ξ^3 model). We note that the shape distribution of the Gaussian random sphere model is determined based on true shape properties of the dust sample without using such optimizations. This has to be taken into account when the Gaussian random sphere model is compared with the spheroidal-ξ^3 model.

The scattering properties obtained using the Gaussian random sphere model are compared with the results of the spheroidal model for individual sizes. The simulated scattering cross sections and scattering matrices of individual sizes, defined by the particle volume, agree very well for size parameters $x \leqslant 1$. The largest

differences between the scattering cross section simulated using the Gaussian random sphere model and the spheroidal models are found in the size range between $x = 5$ and $x = 10$. In this size range the scattering cross sections of the Gaussian random sphere model agree best with the results of the spheroidal model with an equiprobable shape distribution. The differences between the scattering matrices of the various models tend to increase with increasing particle size. In the size range from $x = 1$ to $x = 6$ the Gaussian random sphere model agrees best with the spheroidal model with an equiprobable shape distribution.

After size-averaging, the simulated scattering matrices are compared with the measured scattering matrix of the feldspar sample. Overall, the spheroidal-ξ^3 model agrees better with the measurement than the Gaussian random sphere model. This is true especially for the quantitative agreement of the phase functions from 120° to 170° and the elements $-F_{12}/F_{11}$ from 60° to 120°. In various respects, the Gaussian random sphere model reflects the light scattering properties predicted by the spheroidal-ξ^0 model, which comprises larger contributions of mildly nonspherical shapes. On the other hand, the Gaussian random sphere model qualitatively renders best the flat shape of the phase function in the range of scattering angles from 100° to 170°, and the F_{22}/F_{11} element from 120° to 170°. These features are characteristic for light scattering by truly irregular mineral dust particles.

The Gaussian random sphere model has been applied especially in order to capture the nonspherical and nonsymmetric nature of the particle shapes. However, the Gaussian random sphere geometry cannot reproduce the sharp edges and the flat surfaces of the feldspar particles that are observed on microscopic images. This may explain partly why light scattering predicted by the Gaussian random sphere model shows similarities with light scattering of more mildly nonspherical shapes in various respects. Furthermore, we cannot rule out completely that the shape statistics extracted from the microscope images is biased due a preferential orientation of the particles on the object carrier or due to the fact that the small particles that dominate the size distribution of the sample are under-represented in the shape analysis. Such a bias may be responsible for a mismatch between the simulations using Gaussian random spheres and the measurement.

The light scattering simulations shown in this study are based on the assumption that the particles can be modeled using homogeneous model particles with simplified shapes. Small-scale structures of the surface and inhomogeneities in the volume of mineral dust particles are thus not accounted for. This may be the cause for differences between the measurement and the simulations using the spheroids or the Gaussian random sphere model. Until light scattering by true mineral aerosols can be reproduced accurately by models, light scattering measurements remain a benchmark relevant for further developments.

Acknowledgements

Thanks are due to Alfons Hoekstra, Computational Science Section, University of Amsterdam, for kindly providing computational capacities for the extensive DDA calculations. We would like to thank Karri Muinonen, Observatory, University of Helsinki, for providing the shape generation software for the Gaussian random sphere model.

References

[1] Holben BN, et al. A federated instrument network and data archive for aerosol characterization. Remote Sensing Environ 1998;66:1–16.
[2] Kaufman YJ, Tanré D, Bouché O. A satellite view of aerosols in the climate system. Nature 2002;419:215–23.
[3] D'Almeida GA, Koepke P, Shettle EP. Atmospheric aerosol global climatology and radiative characteristics. Deepak Publ.; 1991.
[4] Mishchenko MI, Lacis AA, Carlson BE, Travis LD. Nonsphericity of dust-like tropospheric aerosols: implications for aerosol remote sensing and climate modeling. Geophys Res Lett 1995;22:1077–80.
[5] Kahn R, West R, McDonald D, Rheingans B, Mishchenko MI. Sensitivity of multi-angle remote sensing observations to aerosol sphericity. J Geophys Res 1997;102:16861–70.
[6] Kalashnikova O, Sokolik I. Importance of shape and composition of wind-blown dust particles for remote sensing at solar wavelengths. Geophys Res Lett 2002;29:10.1029/2002GL014947.
[7] Kahnert M, Kylling A. Radiance and flux simulations for mineral dust aerosols: assessing the error due to using spherical or spheroidal model particles. J Geophys Res 2004;109: 10.1029/2003JD004318, errata: 10.1029/2004JD005311.
[8] Bohren CF, Huffman DR, editors. Absorption and scattering of light by small particles. New York: Wiley; 1983.

[9] Mishchenko MI, Travis LD, Lacis AA. Scattering, absorption, and emission of light by small particles. New York: Cambridge University Press; 2002.
[10] Muinonen K, Nousiainen T, Fast P, Lumme K, Peltoniemi JI. Light scattering by Gaussian random particles: ray optics approximation. JQSRT 1996;55:577–601.
[11] Nousiainen T, Muinonen K, Räisänen P. Scattering of light by large Saharan dust particles in a modified ray-optics approximation. J Geophys Res 2003;108.
[12] Nousiainen T, McFarquhar GM. Light scattering by quasi-spherical ice crystals. J Atmos Sci 2004;61:2229–48.
[13] Klein C. Manual of mineral science, 22nd ed. New York: Wiley; 2002.
[14] Hansen JE, Travis LD. Light scattering in planetary atmospheres. Space Sci Rev 1974;16:527–610.
[15] Huffman DR. The interaction of light with a small-particle system. Adv Phys 1977;26:129–30.
[16] Sokolik IN, Toon OB. Incorporation of mineralogical composition into models of the radiative properties of mineral aerosol from UV to IR wavelengths. J Geophys Res 1999;104:9423–44.
[17] Dubovik O, et al. Variability of absorption and optical properties of key aerosol types observed in worldwide locations. J Atmos Sci 2002;59:590–608.
[18] Tratt DM, Frouin RJ, Westphal DL. April 1998 Asian dust event: a southern Californian perspective. J Geophys Res 2001;106:18371–9.
[19] Maring H, Savoie DL, Izaguirre MA, Custals L, Reid JS. Mineral dust aerosol size distribution change during atmospheric transport. J Geophys Res 2003;108:1–6 [PRD8].
[20] Volten H, Muñoz O, Rol E, de Haan JF, Vassen W, Hovenier JW, Muinonen K, Nousiainen T. Scattering matrices of mineral particles at 441.6 nm and 632.8 nm. J Geophys Res 2001;106:17375–401.
[21] Muñoz O, Volten H, de Haan JF, Vassen W, Hovenier JW. Experimental determination of scattering matrices of randomly-oriented fly ash and clay particles at 442 and 633 nm. J Geophys Res 2001;106:833–44.
[22] Mishchenko MI. Light scattering by randomly oriented axially symmetric particles. J Opt Soc Am A 1991;8:871–82.
[23] Nousiainen T, Vermeulen K. Comparison of measured single-scattering matrix of feldspar particles with *T*-matrix simulations using spheroids. JQSRT 2003;79–80:1031–42.
[24] Veihelmann B, Volten H, van der Zande WJ. Light reflected by an atmosphere containing irregular mineral dust aerosol. Geophys Res Lett 2004;31:1–4 [L04113], 10.1029/2003GL018229.
[25] Nousiainen T, Kahnert M, Veihelmann B. Light scattering modeling of small feldspar particles using simplified shapes. JQSRT 2005, in press.
[26] Kahnert M, Nousiainen T, Veihelmann B. Spherical and spheroidal model particles as an error source in aerosol climate forcing and radiation computations: a case study for feldspar aerosols. J Geophys Res 2005; 110, doi:10.1029/2004JD005558.
[27] Muinonen K. Light scattering by stochastically shaped particles. In: Mishchenko MI, Hovenier JW, Travis LD, editors. Light scattering by nonspherical particles. San Diego: Academic Press; 2000. p. 323–52.
[28] Muinonen K. Introducing the Gaussian shape hypothesis for asteroids and comets. Astron Astrophys 1998;332:1087–98.
[29] Draine BT, Flatau JP. Discrete-dipole approximation for scattering calculations. J Opt Sci Am A 1994;11:1491–9.
[30] Wriedt T, Doicu A. Formulation of the extended boundary condition method for three-dimensional scattering using the method of discrete sources. J Modern Optics 1998;45:199–214.
[31] Purcell EM, Pennypacker CR. Scattering and absorption of light by nonspherical dielectrical grains. Astrophysical J 1973;186:705–14.
[32] Draine BT, Flatau JP. User Guide for the Discrete Dipole Approximation Code DDSCAT 6.1; 2004, <http://arxiv.org/abs/astro-ph/0309069>.
[33] Hovenier JW, van der Mee CVM. Basic relationships for matrices describing scattering by small particles. In: Mishchenko MI, Hovenier JW, Travis LD, editors. Light scattering by nonspherical particles: theory, measurements, and applications. San Diego: Academic Press; 2000. p. 61–85.
[34] Hovenier JW, van der Mee CVM. Testing scattering matrices: a compendium of recipes. JQSRT 1996;55:649–61.
[35] Min M, Hovenier JW, de Koter A. Scattering and absorption cross sections for randomly oriented spheroids of arbitrary size. JQSRT 2003;79:939.
[36] Mishchenko MI, Macke A. How big should hexagonal ice crystals be to produce halos? Appl Opt 1999;38:1626–9.
[37] Liu L, Mishchenko MI, Hovenier JW, Volten H, Muñoz O. Scattering matrix of quartz aerosols: comparison and synthesis of laboratory and Lorenz–Mie results. JQSRT 2003;79–80:911–20.
[38] Volten H, Muñoz O, Hovenier JW, de Haan JF, Vassen W, van der Zande WJ, et al. WWW scattering matrix database for small mineral particles at 441.6 nm and 632.8 nm. JQSRT 2005;90:191–206.